Detection of the bright band with a vertically pointing k-band radar

Thomas Pfaff[*], Alexander Engelbrecht and Jochen Seidel

Institute for Modelling Hydraulic and Environmental Systems, Stuttgart, Germany

Abstract

Quantitative precipitation estimation based on weather radar data suffers from a variety of errors. During stratiform events, a region of enhanced reflectivity, called the bright band, leads to large positive biases in the precipitation estimates when compared with ground measurements. The identification of the bright band is an important step when trying to correct weather radar data for this effect. In this study we investigate three different methods to identify the bright band from profiles measured by a vertically pointing K-Band Micro Rain Radar (MRR). The first tries to fit a piecewise linear function to the profile. The bright band characteristics are then derived from the fitted function parameters. The second uses only reflectivity information, while the third makes additional use of the falling velocity, which is also measured by the MRR. This last method shows the greatest skill in identifying the bright band height, followed by the function fit and the pure reflectivity methods. A comparison with data from a scanning radar shows that the height estimated in this way corresponds well with the bright band features observed in the radar scan.

Keywords: MRR, Bright Band, Vertical Profile of Reflectivity, Falling Velocity, Weather Radar

1 Introduction

The bright band is a zone of high reflectivity which is commonly observed in radar images of widespread precipitation. This phenomenon is caused by the change of aggregate state of hydrometeors from ice to liquid. Battan (1973) states several processes during the passage of the hydrometeors through the melting layer (i.e. around and below the 0 °C isotherm), which lead to the enhancement of the reflectivity signal.

For precipitation estimation, the reflectivity needs to be converted to rainfall intensity using Z/R relationships, which are mainly of the form $Z = aR^b$ (see e.g. Battan (1973) for a list of possible parameters a and b). If the bright band effect is not accounted for before or during Z/R conversion, large positive biases are introduced into quantitative precipitation estimates. Furthermore, for the frozen hydrometeors above the bright band, standard Z/R relationships which assume liquid precipitation do not apply leading to negative biases in this region.

A comprehensive literature review of all major sources of uncertainty including those connected with vertical inhomogeneities of the radar reflectivity factor commonly denoted as 'vertical profile of reflectivity' (VPR), of which the bright band is a special but the most prominent case, is given by Villarini and Krajewski (2009).

There are two basic methods to measure the VPR. The first uses radar scans at different elevation angles.

From this data, the VPR is constructed by taking the data from vertically aligned range bins. This approach allows the acquisition of vertical profiles over a large region, the increasing beam width, however, limits the resolution of these profiles. Additionally, as the individual scans take time to complete, the profiles generated from these data do not represent instantaneous snapshots and may be affected by advection and the evolution of the precipitation field.

The second method uses a vertically pointing radar. This way, the VPR can be measured instantaneously with very high vertical and temporal resolution, even though the analysis is limited to a single point in space.

As advantages and drawbacks of these two methods are quite complementary, vertically pointing radars may provide useful auxiliary information for the correction of scanning radar data. Towards this goal, the identification of the bright band may be a useful first step. Therefore, in this article we compare three different approaches to detect the bright band from vertically pointing K-band radar data and compare the results to data from a scanning operational C-Band weather radar.

2 Radar systems and study area

The data used in this study was acquired with a Metek Micro Rain Radar (MRR) situated on the premises of the Vaihingen Campus of the University of Stuttgart. It is part of a routinely operated meteorological observation station. Its technical and operating specifications are given in Table 1. The MRR provides drop size and velocity spectra as well as several aggregate values like radar

[*]Corresponding author: Thomas Pfaff, Institute for Modelling Hydraulic and Environmental Systems, Pfaffenwaldring 61, 70569 Stuttgart, Germany, e-mail: thomas.pfaff@iws.uni-stuttgart.de

Table 1: Operating characteristics of the MRR at the meteorological station of the study area.

Emission frequency	24 GHz (K-Band)
Transmit power	50 mW
Receiver-transmitter-	Shifted parabolic antenna,
Antenna diameter	0.6 m
Beam width (3 dB)	2 °
Modulation	FMCW (frequency modulated continuous wave)
Height resolution	100 m
Averaging time	60 s
Height range	3100 m
Measured variable	Averaged power spectra of the received signal
Location	48.74 N 9.10 E
Elevation	453 m a.s.l.

reflectivity, rain intensity and reflectivity weighted average falling velocity, which are derived from the spectral information. In this study, radar reflectivity and average falling velocity were used by the different algorithms.

According to the manufacturer of the MRR, the lowest two levels of the data are not reliable. In addition, it was found that also the top two levels showed continuously larger reflectivity estimates than the levels below. Therefore the two levels at the top and the bottom of each profile were removed from all analyses.

The scanning radar data used in this study is the DX product from the German Meteorological Service (DWD) operational radar network's station Türkheim (WMO-ID 10832, located at 48 ° 35′ 10″ N 9 ° 47′ 02″ E). At the time of data acquisition for this study, it was a C-Band, single-polarization, Doppler radar doing a precipitation scan every 5 minutes. These scans have an azimuthal resolution of 1 ° and a range resolution of 1 km with an unambiguous range of 128 km.

One specialty of the DWD DX product is that for these particular scans the antenna elevation is not kept constant. In order to get the lowest possible precipitation estimate that is not affected by partial or full shielding, the antenna elevation is configured to vary azimuthally following the horizon. Therefore, bright band effects will not show the usually known circular features but will appear at different ranges for a number of sectors depending on the elevation pattern of the particular radar.

Two periods were analyzed, which show distinctly different characteristics. The first, ranging from 2011-12-16 01:40 CET to 2011-12-17 00:00 CET observes the passage of a winter storm. Fig. 1a shows the measured reflectivity profiles as well as 10 minute ground precipitation accumulations measured by a co-located weighing rain gage. The bright band can be seen to vary between 400 and 1300 m above ground level with a decrease in height in the afternoon due to the passage of a cold front.

The second period is from 2012-06-13 00:30 CET to 2012-06-13 08:30 CET where a chain of low pres-
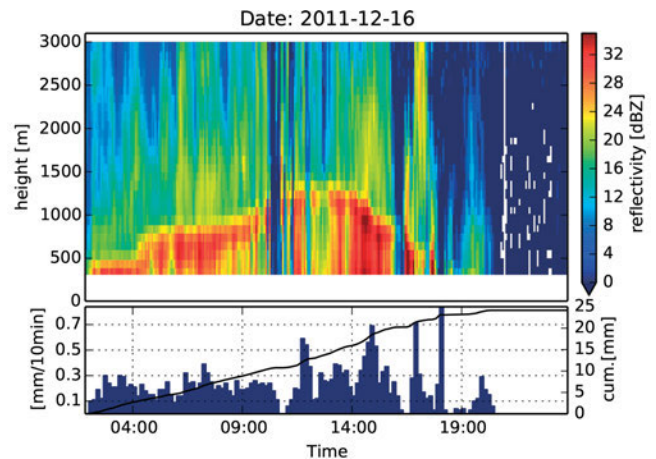
(a) Period 1 – winter storm.
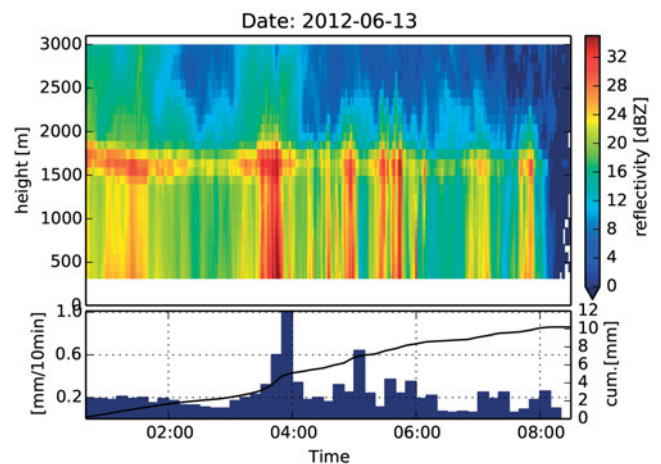
(b) Period 2 – summer rainfall.

Figure 1: Temporal evolution of vertical profiles and ground precipitation for two studied periods.

sure systems over central Europe lead to widespread and in parts intense precipitation including small thunderstorms. The reflectivity plot in Fig. 1b shows a bright band at a relatively constant height of about 1700 m above ground level.

3 Methodology

First, the three bright band detection algorithms are presented, followed by the methods and parameters used to assess their performance. Finally, a comparison of MRR-detected bright band heights with two-dimensional radar data is presented.

3.1 VPR model

One approach used in this study was to fit an analytical function to the observed data. With this method it would not only be possible to infer the bright band peak and thickness, but to model the vertical profile for any height level.

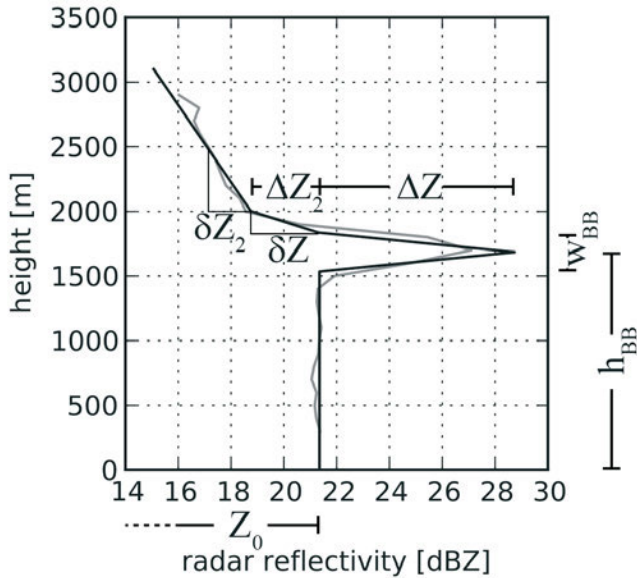Similar to KITCHEN et al. (1994) a piecewise linear formulation of the VPR was used in this analysis.

Figure 2: Schematic indicating parameters used in Function Fit.

It assumes that the reflectivity below the bright band is constant Z_0. The bright band itself is characterized by three parameters: the reflectivity increase of the bright band peak ΔZ, the bright band peak height h_{BB} and the thickness w_{BB}. The bright band peak is assumed to be in the center. Therefore, the bright band bottom is defined as $h_{BB,1} = h_{BB} - w_{BB}/2$, and accordingly the top is at $h_{BB,2} = h_{BB} + w_{BB}/2$. The upper part of the VPR is divided into two regions. In the first, the reflectivity decreases with height at a rate of δZ [dB/m] up to h_1, which is defined as the height where the reflectivity is reduced by ΔZ_2. From this point on the reflectivity linearly decreases at a rate of δZ_2 [dB/m]. Eqn. 3.1 gives the mathematical representation of this VPR function, while Fig. 2 shows an example of a measured and a fitted profile together with schematic depictions of the respective parameters.

$$vpr(h) = \begin{cases} Z_0, & \text{if } 0 \le h < h_{BB,1} \\ Z_0 + \Delta Z \cdot \frac{h - h_{BB,1}}{w_{BB}/2} & \text{if } h_{BB,1} \le h < h_{BB} \\ Z_0 + \Delta Z \cdot \frac{h_{BB,2} - h}{w_{BB}/2} & \text{if } h_{BB} \le h < h_{BB,2} \\ Z_0 - \delta Z \cdot (h - h_{BB,2}) & \text{if } h_{BB,2} \le h < h_1 \\ Z_0 - \Delta Z_2 - \delta Z_2 \cdot (h - h_1) & \text{if } h > h_1 \end{cases}$$
(3.1)

Due to the considerable number of parameters, the optimization is very dependent on a good choice of starting values. In order to enable the optimization to adapt to changes in the VPR over time, if the current optimization converged, its results were used as starting values for the optimization of the following profile. If it did not converge, the original starting values were used again in the next run. The first set of starting parameters for each of the analyzed periods was determined manually.

3.2 Method using reflectivity gradient

CHA et al. (2009) used vertical gradients in the reflectivity profile measured by a MRR to determine bright band bottom and top. The bottom (H_B) and top (H_T) were defined as the height levels of largest positive and negative reflectivity gradient, respectively. The height of the maximum reflectivity in the whole profile was determined to be that of the bright band peak. If this height was not between H_B and H_T the profile was excluded from the analysis, i.e. assumed to be without a bright band.

A sharpness constraint was employed to ensure that a sufficiently visible bright band was detected. This sharpness was defined as the ratio $\frac{\Delta Z}{BB_{th}}$, where $\Delta Z = [Z_{peak}/Z_{rain} + Z_{peak}/Z_{snow}]/2$. Z_{rain}, Z_{peak} and Z_{snow} are the reflectivity factors just below, at the peak and just above the bright band, respectively. BB_{th} is the bright band thickness defined as the difference between top and bottom height levels.

This method had been devised with the purpose of selecting vertical profiles suitable for an analysis of different rainfall generation processes. Therefore the focus was not on stability and robustness of the method and it was not tested with regard to these criteria.

3.3 Method using falling velocity

A third approach uses the average falling velocity to bound the search for the maximum reflectivity. As described e.g. in BATTAN (1973), the falling velocity of the hydrometeors increases in the melting layer.

As the maximum reflectivity in the bright band appears in a region where not all ice phase hydrometeors have melted completely, it can be expected that the falling velocity will still increase below the reflectivity peak before reaching a maximum velocity.

WHITE et al. (2002) used Doppler signal to noise ratio (SNR) and average falling velocity to determine the bright band height. In this study, the radar reflectivity factor is used instead of SNR – as it shows essentially the same behavior and SNR was not available – together with the falling velocity, with a slightly modified algorithm. With this data, the approach to determine the bright band peak using falling velocity as auxiliary information proceeds as follows.

1. normalize the velocity profile between 0 (minimum velocity) and 1 (maximum velocity)

2. determine the highest level at which the velocity exceeds a threshold for the last time. In this study 0.8 was chosen, based on visual inspection of the normalized velocity profiles.

3. starting from there, look for the height level of the maximum reflectivity

3.4 Goodness of detection parameters

For both observation periods in all reflectivity profiles the bright band peak height was determined manually. This provided the reference data set for comparison. For all three identification algorithms goodness of detection parameters were calculated using the contingency table approach. The four categories were defined as follows:

- A hit is counted if the estimated bright band peak height is within tolerance of the reference peak height.
- A miss is counted if no bright band peak height is detected although the reference identified a bright band peak.
- A false alarm is counted if the estimated bright band peak height is outside the tolerance of the reference peak height, or if there is an estimate but no bright band was observed in the reference.
- A correct negative is counted if both estimation and reference did not identify a bright band.

From these categories the parameters "false alarm ratio" (FAR), "probability of detection" (POD), "success ratio" (SR), "critical success index" (CSI) and identification bias (BIAS) were calculated as follows:[1].

$$FAR = \frac{\text{false alarms}}{\text{hits + false alarms}}$$
$$POD = \frac{\text{hits}}{\text{hits + misses}}$$
$$SR = \frac{\text{hits}}{\text{hits + false alarms}} = 1 - FAR$$
$$CSI = \frac{\text{hits}}{\text{hits + misses + false alarms}}$$
$$BIAS = \frac{N_{fc}}{N_{\text{obs}}} = \frac{\text{hits + false alarms}}{\text{hits + misses}} \qquad (3.2)$$

For both the VPR-model and the falling velocity method a simple filter was used to determine periods without bright band. Profiles with a mean reflectivity below 10 dBZ were ignored by the algorithm and therefore considered to be without bright band. In addition, for the VPR-model the convergence criterion of the optimization algorithm was evaluated. If the optimization did not converge, the respective profile was also considered as a non-detection.

The combination of these parameters will be displayed in a so-called performance diagram (ROEBBER, 2009), which allows a concise and objective assessment of the overall performance of the individual algorithms.

3.5 Comparison with scanning radar

In the last step the qualitative effect of the bright band on two-dimensional radar images was investigated. To show this effect, bright band bottom, peak and top
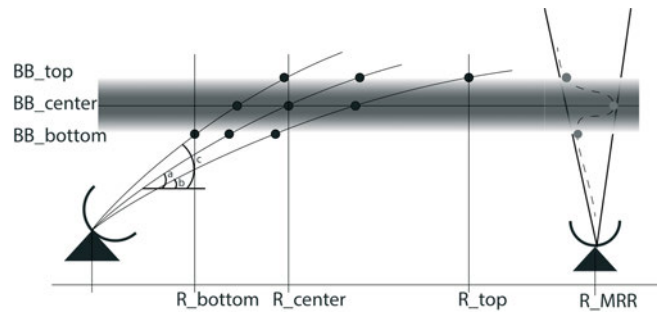

Figure 3: Schematic depiction of the intersection of the radar beam with the bright band.

height were determined from MRR profiles and their apparent range in the radar image was calculated taking the azimuthally variable elevation angles into account. Bright band top and bottom were defined as the heights where the reflectivity had dropped by 3 dB from that of the bright band peak. Similarly, a 3 dB beam width of 1° was assumed to calculate the intersections between beam and bright band (which are shown schematically in Fig. 3).

4 Results

At first, the results of bright band peak identification will be presented for the two newly introduced detection methods directly in comparison with the original reflectivities. This is done in order to give the reader the possibility to assess the overall stability and behavior of these approaches before presenting summary performance measures.

The bright band peak heights determined by the VPR-model are shown in Fig. 4. The estimates follow the development of the maximum reflectivity very closely. The first period poses more challenges to this approach due to several properties of the profile evolution. The cutoff at low elevations leads to the problem that, at the beginning of the period, the bright band is almost below the minimum detectable height. Here, the optimization leads to bright band peak height estimates that cannot be verified directly by the measurement data. As a second challenge, the measurements are disrupted several times most probably due to the intensity of the storm. Here, the optimization is less able to estimate profiles properly during and shortly after these periods as the starting parameters for the optimization might not be close enough to ensure proper convergence. However, once the measurement is stable again and some profiles have been identified successfully, the further development of the reflectivity profile and the visible decrease in bright band height is captured well.

Figs. 5a and 5b show the bright band peak detection results obtained using the velocity method. For the sake of clarity only every 10th identified height is displayed for period 1 and every fifth for period 2. Apart from a few occasional outliers the maximum reflectivity in the
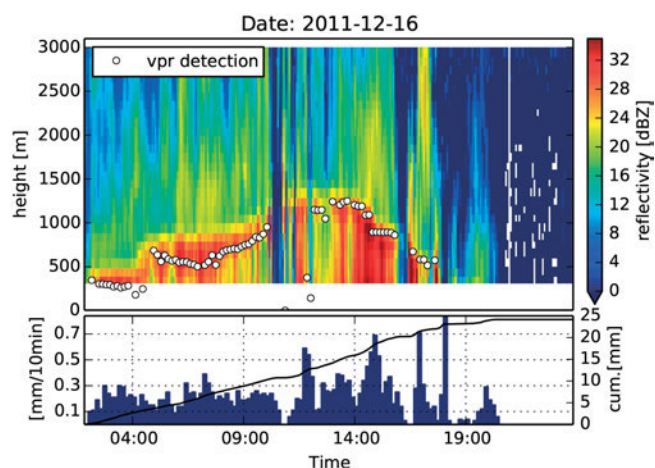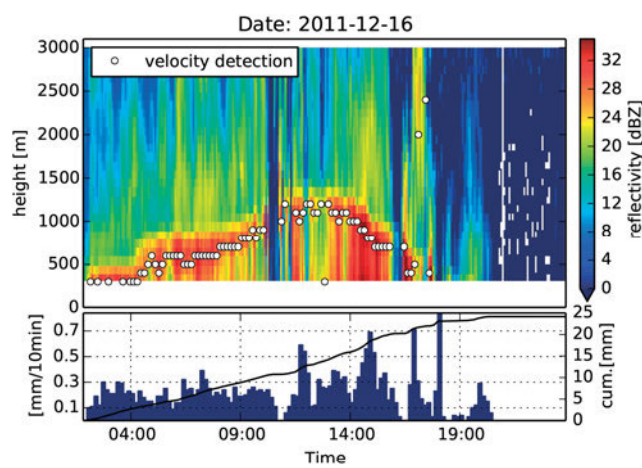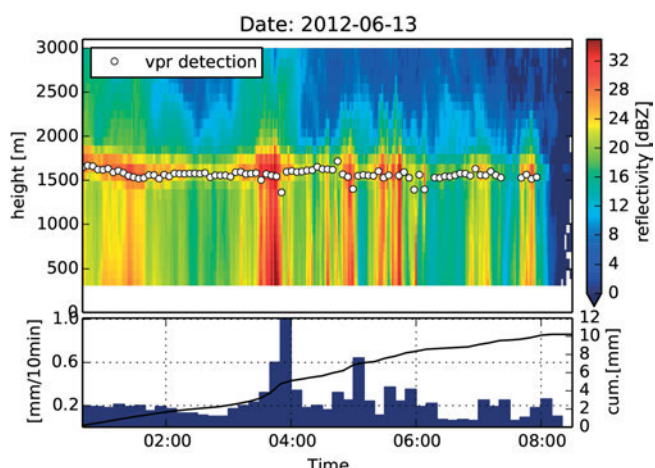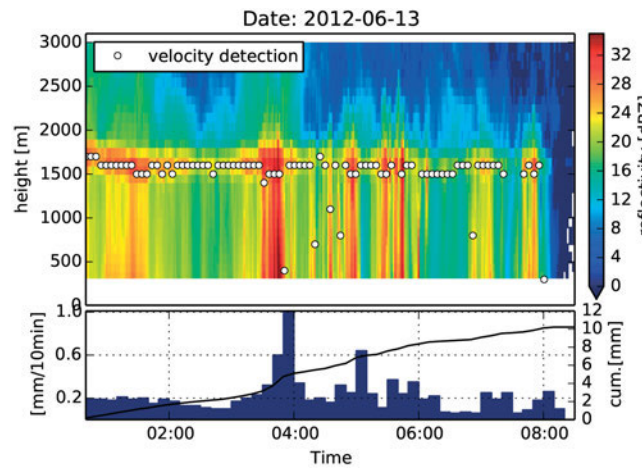
Figure 4: Measured reflectivity profiles and bright band peak heights identified using the VPR-model approach.

Figure 5: Measured reflectivity profiles and bright band peak heights identified using the falling velocity approach.

bright band is detected reliably even if the bright band height changes rapidly over time as seen in Fig. 5a. The method appears to be more robust than the VPR-model method in the sense that it is able to detect bright band signatures even shortly before and after the missing data in period 1. On the other hand, in the later stages of period 1 and sporadically throughout period 2, the detection diverges considerably from the perceived bright band height, and here the VPR-model method shows a more stable behavior.

The results of the identification based on the algorithm presented by CHA et al. (2009) are given in Fig. 6. This method also appears to detect the bright band correctly most of the time with only few outliers. The major difference to the other two methods is that there are more periods, where the algorithm does not produce any estimate of the bright band height.

Before presenting the derived parameters, Fig. 7 shows the relative frequencies of the four possible outcomes of the comparison between manual and algorithmic identification of the bright band height.

For each of the three tested methods, two results are presented for each period. The first, given the subscript 0

counts a hit only, if the exact height level as identified manually is predicted by the algorithm. This is directly applicable for the velocity and CHA et al. (2009) methods, which work with the discrete height levels of the MRR data. As the VPR-model produces non-integer height level estimates, these were rounded to the nearest integer. MITTERMAIER and ILLINGWORTH (2003) state that an error of not more than 200 m in estimated bright band height would be permissible in an operational setting, the second set of results allows for a deviation between reference and estimated height of ±100 m. Here, the fractional heights given by the optimization can be used directly, while it translates to allowing a deviation of one integer height level for the other two methods.

In Fig. 7a, both velocity and VPR-model method show a similar number of correct negatives. This is due mostly to the fact that the majority of the successful non-detects is caused by the mean 10 dBZ filter applied to these two methods. As the CHA et al. (2009) method had its own way to determine non-detections, its relative amount differs. The number of hits is largest for the velocity method, with a very small ratio of misses, i.e. there is a small bias toward identifying too many bright
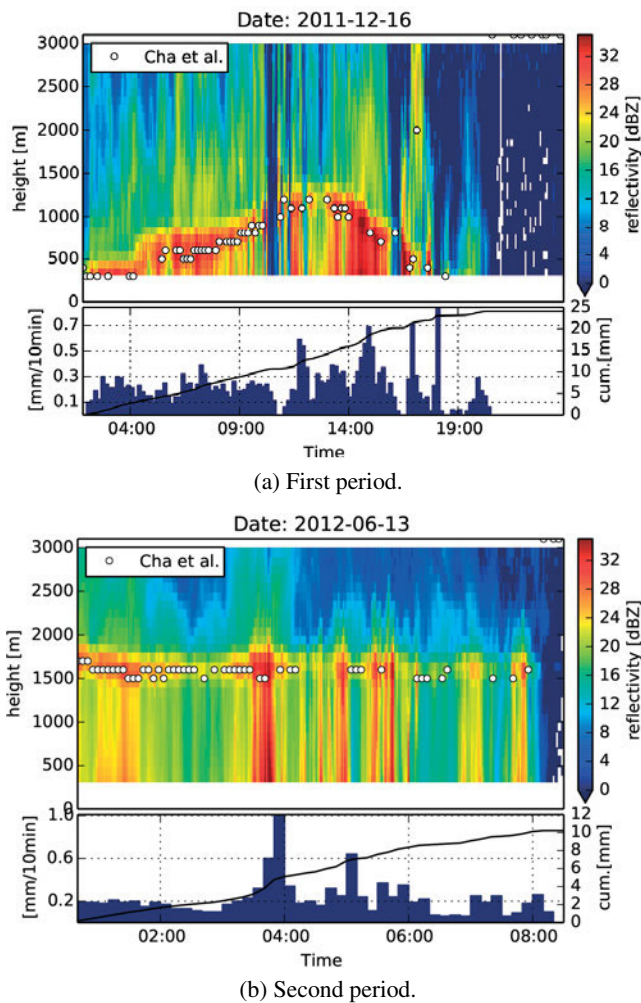
(a) First period.

(b) Second period.

Figure 6: Measured reflectivity profiles and bright band peak heights identified using the approach by CHA et al. (2009).

bands. The VPR-model method shows both more misses as well as false alarms, so, while appearing reasonable and more stable in Fig. 4 than those of the velocity method, the estimates are slightly more often too far off.

This is a problem inherent to this fitting-by-optimization method. While Fig. 2 shows a measured profile that is very nicely approximated, even there, a strong overestimation of bright band peak reflectivity occurs in order to allow for a least squares optimal fit of the whole curve. In other profiles, the compromise may lead to the bright band height to be estimated away from the measured one.

While the method of CHA et al. (2009) performs slightly better than the VPR-model approach concerning hits, there is both a greater number of misses and false alarms, mainly due to the algorithm estimating bright band heights even for profiles, which are not raining. Allowing for some tolerance has the largest effect on the results of the VPR-model method, while the other two show only marginal improvements.

In the second period (Fig. 7b), all profiles had a detectable bright band and therefore there are no profiles in the category 'correct negative'. In this period all methods profit from an increased tolerance.
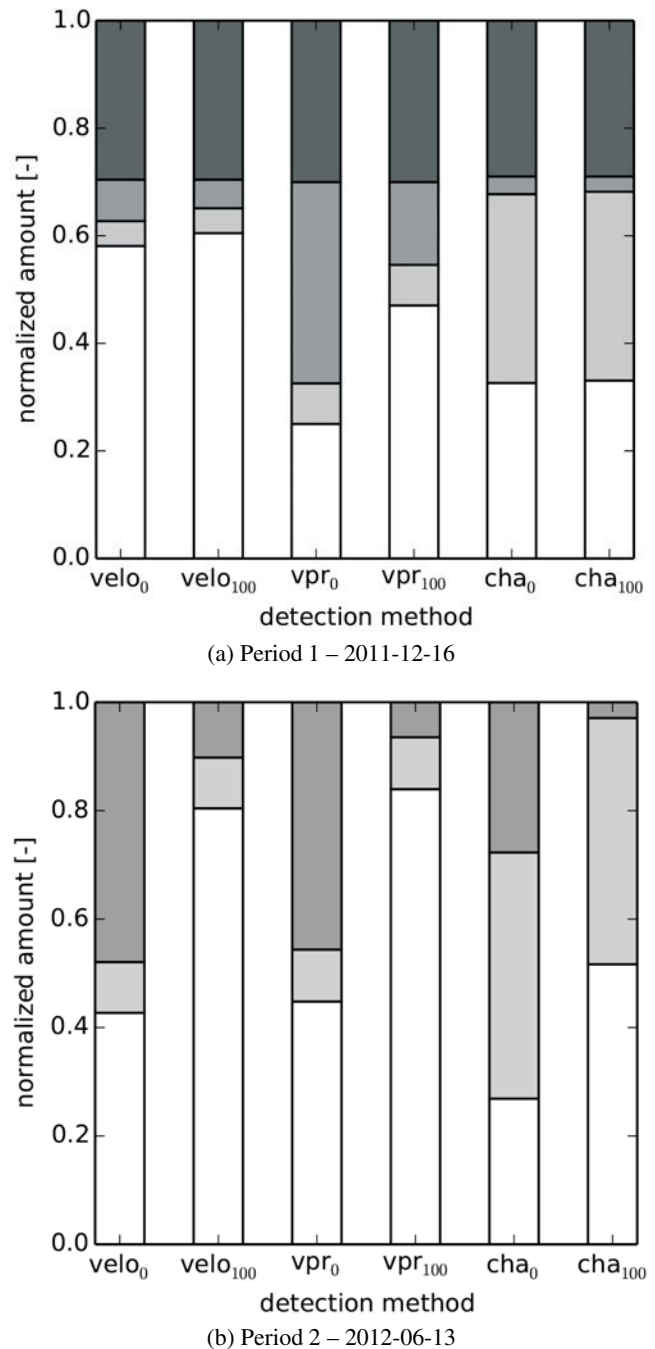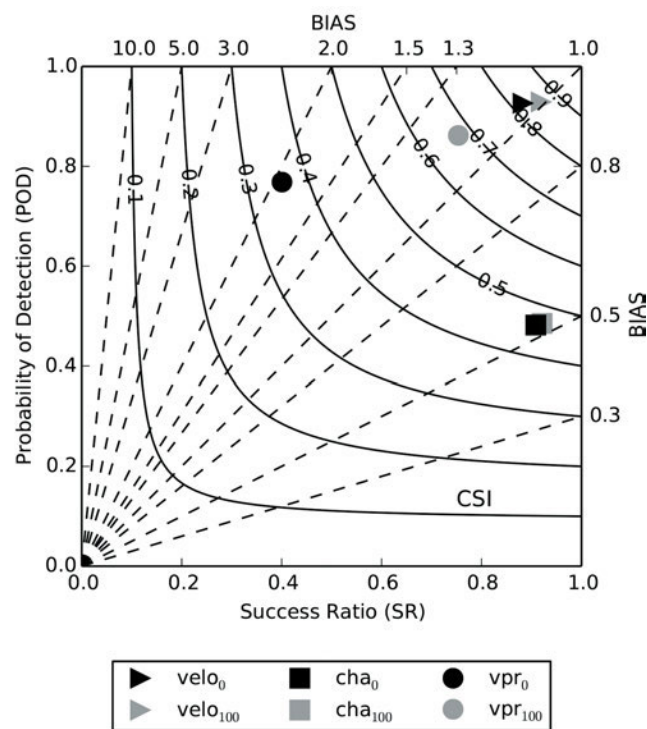

(a) Period 1 – 2011-12-16

(b) Period 2 – 2012-06-13

Figure 7: Bar plots showing the relative amounts of hits (white), misses (light gray), false alarms (dark gray) and correct negatives (black) for the different approaches. The subscripts 0 and 100 indicate the tolerance in m in bright band height allowed for a hit to be scored.

While these results may already give an impression of the performance and accuracy of the individual methods, these can be even more concisely displayed using the performance diagram introduced by ROEBBER (2009). Plotting success ratio ($SR = 1 - FAR$) and probability of detection (POD) on the *x*- and *y*-axes respectively, together with isolines of BIAS and critical success index (CSI) that can be derived from these two measures, the quality of each method and possible biases can be more easily estimated visually.

(a) Period 1 – 2011-12-16
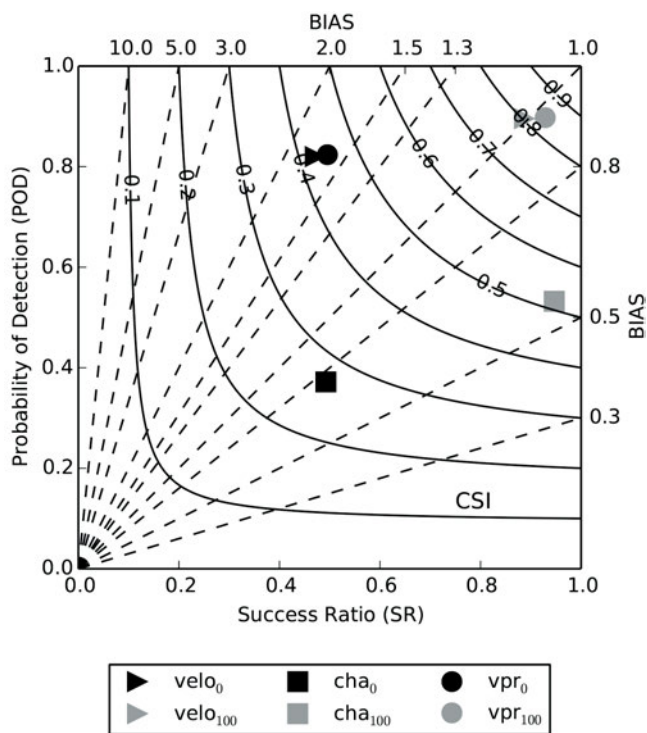
(b) Period 2 – 2012-06-13

Figure 8: Performance diagrams.

Figure 9: Precipitation scan of Radar Türkheim 2011-12-16 11:50 CET with bright band delineations (solid white: R_center, dashed white: R_bottom and R_top, according to Fig. 3) determined from MRR measurements. The white circle indicates the location of the MRR.

Fig. 8a shows that for period 1 all algorithms tend to be overconfident with their detections, and that both CHA et al. (2009) and velocity methods produce estimates that are either correct or much farther off than the allowed 100 m tolerance. The velocity method produces CSIs above 0.8 with almost no bias.
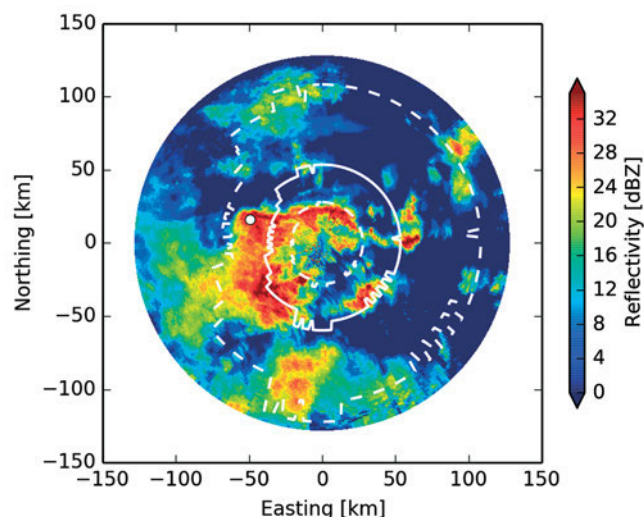
In period 2, as presented in Fig. 8b, the methods are less accurate, missing the exact height of the bright band in about 40 % of all analyzed profiles, but most estimates are within the 100 m tolerance as displayed by the marked improvement of all statistics.

To summarize, the VPR-model and the velocity approach perform very well in both periods while the method of CHA et al. (2009) would have to be augmented by some additional constraint or information to produce reliable bright band estimates.

Looking at the influence of the bright band on scanning radar imagery, a scan of the DWD radar station Türkheim during period 1 was overlayed by the estimated locations of the radar beam traversing the bright band. Fig. 9 shows bright band bottom, center and top as calculated based on Fig. 3.

First, the varying positions of the individual bright band intersection locations should be noted, which are due to the aforementioned variable elevation angles of this particular data product. Second, most of the enhanced reflectivity in the image would have to be attributed to bright band interference. Especially in the region south of the MRR position in the sector between 200 and 300 ° the highest reflectivities coincide with the estimated bright band center. Third and maybe most disturbingly, even with the very narrow definition of 3 dBZ bright band width and 3 dBZ beam width, the region of possible bright band interference covers a major part of the image.

5   Conclusions

This study presented a comparison between three different methods to determine bright band height from observations by a vertically pointing radar.

It appears that the approach based on the reflectivity and falling velocity profile produces the best results. If only reflectivity were available, fitting even a very simplified theoretical profile may be preferable to algorithms that rely on gradients and other properties of the profile only.

While the profile fitting method produced good results when the bright band height only was concerned, further investigations would be needed to assess, whether the additional information, provided by the rest of the fitted profile would be accurate enough to allow for a quantitative correction based on point scale, measured vertical profiles.

Given the large areas that might be contaminated by bright band influences when using radar scans taken at small elevation angles, a correction seems to be absolutely necessary to avoid biases in long term precipitation accumulations.

This case study focused on investigating the performance of different algorithms during periods where a bright band was visible. Applying any of these in an operational setting would require some additional tests. First of all, the test dataset would have to be extended and should especially include periods with precipitation but without a bright band. While the mean 10 dBZ criterion employed in this study has proved sufficient for the cases presented here, it needs to be verified, and most probably extended for operational use. Also, right now, the MRR profiles were taken as they were. As with any remote sensing technique the reflectivities obtained by the MRR are subject to a variety of errors. Tilted rain shafts may introduce spurious effects on the instantaneous VPR. Additional research would be required to estimate the magnitude of such effects. In this study, 'attenuation corrected' reflectivity as supplied by the MRR software was used. During periods of intensive precipitation, attenuation will become a problem due to the high frequency of the radar waves. Although it may be hoped that events like these will be caused mainly by convective precipitation, where the bright band may not be a problem for precipitation estimates by scanning radar, these profiles will nevertheless be dangerous to interpret.

A direct correction of scanning radar reflectivities based on the VPR measurements made by the MRR was not attempted for several reasons. First, the measurement takes place at one location only. Given the temporal evolution of the VPR in the first period it would need additional information to regionalize the measured profiles or bright band heights. Without that, a correction will most probably fail. Second, a relation between reflectivities obtained by the MRR and those of the scanning radar needs to be defined. Preliminary research into this problem showed that, while the correspondence between both is high, there is considerable spread up to 20 dBZ. This may be due to the different volumes sampled by both radars, deviations in measurement height, caused by propagation conditions differing from those of a standard atmosphere, which were assumed here, attenuation effects on the side of the scanning radar and many others.

6 Acknowledgments

References

Battan, L.J., 1973: Radar observation of the atmosphere. – The Univ. of Chicago Press, 324 pp.

Cha, J.-W., K.-H. Chang, S.S. Yum, Y.-J. Choi, 2009: Comparison of the Bright Band Characteristics Measured by Micro Rain Radar (MRR) at a Mountain and a Coastal Site in South Korea. – Adv. Atmos. Sci. **26**, 211–221.

Kitchen, M., R. Brown, A. Davies, 1994: Real-time correction of weather radar data for the effects of bright band, range and orographic growth in widespread precipitation. – Quart. J. Roy. Meteor. Soc. **120**, 1231–1254.

Mittermaier, M.P., A.J. Illingworth, 2003: Comparison of model-derived and radar-observed freezing-level heights: Implications for vertical reflectivity profile-correction schemes. – Quart. J. Roy. Meteor. Soc. **129**, 83–95.

Roebber, P.J., 2009: Visualizing Multiple Measures of Forecast Quality. – Wea. Forecast. **24**, 601–608.

Villarini, G., W.F. Krajewski, 2009: Review of the Different Sources of Uncertainty in Single Polarization Radar-Based Estimates of Rainfall. – Surveys Geophys. **31.**, 107–129.

White, A.B., D.J. Gottas, E.T. Strem, F.M. Ralph, P.J. Neiman, 2002: An automated brightband height detection algorithm for use with Doppler radar spectral moments. – J. Atmos. Ocean. Technol. **19**, 687–697.